Observations of Transient Flooding in a Proton Exchange Membrane Fuel Cell Using Time-Resolved Neutron Radiography

M. A. Hickner,[a] N. P. Siegel,[b] K. S. Chen,[c] D. S. Hussey,[d] and D. L. Jacobson[d]

[a]Department of Materials Science and Engineering, The Pennsylvania State University, University Park, PA 16802.
[b]Energy, Resources & Systems Analysis Center, and [c]Engineering Sciences Center, Sandia National Laboratories, Albuquerque, New Mexico 87185, USA.
[d]NIST Center for Neutron Research, National Institute of Standards and Technology, Gaithersburg, Maryland 20899-8461, USA.

Abstract

The generation and transport of water in both the liquid and gas phases during device operation is an important area of study to understand both steady-state and transient performance of proton exchange membrane fuel cells. Specifically, localized high concentrations of liquid water within the cell can cause flooding, which leads to decreases in cell performance, localized fuel starvation and degradation, or in extreme cases, collapse of the cell output. A variety of experimental and simulation techniques have been used to elucidate flooding events, yet, a comprehensive understanding of what leads to flooding and the specific details of how flooding affects fuel cell performance, especially during transient operational modes, have not been completely developed. The work reported here couples both direct observation of liquid water flooding, primarily in the gas flow channel, with measurements of cell performance, outlet temperature, and outlet dew point during a step change in current density. The evolution of the water buildup and water slug dynamics was monitored as well as the transient temperature and electrical performance of the cell in real time. This investigation is useful in that both the

size and location of the water slugs and the cell performance can be connected to describe how the liquid water influences cell operation.

Introduction

Flooding of proton exchange membrane fuel cells by liquid water is currently one of the most critical research topics in applied fuel cell research. As the current density of PEMFCs increases due to improvements in materials, operating strategies, component and cell fabrication techniques, proper water and thermal management becomes crucial to maintaining durability and high performance over a wide range of operating conditions. Many modeling and experimental investigations have explored the concept of flooding over a wide experimental space, but no unified picture of liquid water transport and the factors that lead to flooding currently exists. As a consequence of the lack of fundamental understanding in this area, and dearth of detailed experimental data concerning coupled cell performance and water saturation measurements, the concept of flooding itself is ill-defined. There may be flooding in the catalyst layers, the gas diffusion layer (microporous or macroporous layers), or the gas flow channel[1] and it is often not clear which regime is being probed experimentally if channel-level and cell-level data on liquid water content are not available. Additionally, many fuel cell practitioners will point to the effects of "flooding" as a cause of mass transport limitations, however as was demonstrated previously,[2] not all mass transport limitations can be ascribed to flooding by liquid water.

Past studies have successfully employed neutron radiography to image the liquid water content in operating PEMFCs.[3,4] Most of the work reported to date has dealt with measuring the steady-state water content distribution across the active area of the cell and more recently, the steady-state water distribution through the thickness plane of the MEA.[2] Due to the rapid increase in the sophistication of diagnostic and simulation tools, especially neutron[5,6] and x-ray[7] radiography and advanced two-phase simulation strategies,[8,9] there is significant information on the steady-state distribution of liquid water and local conditions across the cell active area. These distributions are a result of reactant consumption, water generation and condensation, local current density variations, land/channel boundaries, and other effects that are determined by the local conditions and geometric constraints in the cell that can vary on the scale of millimeters to micrometers.

Researchers are now turning their attention to characterizing and describing transient phenomena of fuel cell devices that occur during changes in current density, temperature, gas flow rates, inlet relative humidity, and changes in cell load.[10,11,12,13] Experimental investigations of large-scale hardware interactions have been conducted by Moore, et al.[10] The hardware-in-loop concept is a valuable tool to probe fuel cell system interactions. The authors of this study observed that current and gas flow transients followed the set points with high accuracy, but no information was given on the cell potential transients or outlet gas conditions, which would have given some clues as to the performance and internal state of the fuel cell itself. Maranzana, et al.,[11] measured

temperature, current, and pressure drop transients in a transparent cell. This report is interesting in that the local and global behavior of the cell can be decoupled based on its segmented design. The authors observed time transients of current, temperature and pressure drop on the order of 5-10 min during fuel cell startup, which is in agreement with other studies that assert fuel cells under dynamic operation, despite sometimes rapid electrical transients, can take significant time to achieve a pseudo steady-state.

Gerteisen[12] employed a model to expressly account for transient evolution of saturation as the current density was incremented. The reported simulations show changes in saturation that lagged the current density by times on the order of 40 s. The model incorporated liquid water transport and buildup in both the catalyst layer and the gas diffusion layer. Simulations with transient liquid water buildup were able to explain the flooding hysteresis loop that is often observed in polarization curves when scanning from low to high current densities and back too quickly. Wang and Wang[13] also used simulations to probe the transient response of liquid water in the porous media of a fuel cell and observed in-plane changes in saturation occurring across the gas diffusion layer (GDL) on the time scale of approximately 20 s. While most full-cell models to not explicitly describe the geometry of the pore space and water, there have been very detailed recent reports on the local behavior of liquid water droplets[14,15] and slugs,[16] which help to cement the picture of microscopic processes occurring in the cell, but a full-cell picture of the effects of transient processes on fuel cell behavior is still in its infancy.

Given the porous nature of the fuel cell components, and the above-mentioned experimental insights into the time required to achieve steady operation after a step-change in conditions, it is reasonable to assume that transient processes within and around the porous media of the fuel cell account for some of the observed transient behavior in full-cell experiments. When the power output of the cell is incremented, the electrical response is rather rapid, on the order of 1 s to 2 s or less, owing to fast transport of reactants in the gaseous phase. The slower-time transients in current, if voltage is the controlled output, or voltage, if current is the controlled output, are related to water building up in the porous media and gas channels and local temperature changes, both of which may alter the local water balance, thus affecting the local current density, or cause slow drying or flooding of the whole cell, which is observable on the order of minutes.

As fuel cells are nearing commercialization, transient operation, startup, and load cycling issues are becoming increasingly important from both operational flexibility and degradation prevention points of view. In this paper, transient flooding phenomena are reported across the area of a 50 cm^2 active area fuel cell for two cathode flow conditions at 60 and 80 ºC. Neutron radiographs were recorded every 10 s over the course of 1000 s experiments to determine the liquid water content distribution of the cell during a step change in current from 0 A cm^{-2} to 1.5 A cm^{-2}. The anode and cathode outlet temperatures and dew points were also recorded in addition to the cell performance parameters during the experiment. The goal of this paper is to provide quantitative insight into the relationships between water content, electrical performance, gas

temperature, and gas dew point and highlight the dynamics of the cell that are not accessible by monitoring the electrical performance alone.

Experimental

The imaging instrumentation, experimental fuel cell hardware and test stand, and data analysis routines used in this set of experiments were similar to that reported previously.[17] Co-flow anode and cathode, parallel four-channel serpentine flow fields were employed in 50 cm^2 active area (7.1 cm x 7.1 cm) fuel cell hardware (Fuel Cell Technologies, Albuquerque NM[a]) with edge-heated plates. Experiments were conducted under conditions of constant air flow to the cathode, which was set at a stoichiometric flow rate of two or four for a current density of 1.5 A cm^{-2}. The back pressure on the cell maintained at 50 kPa gauge on both anode and cathode at all times. The anode flow rate was maintained at 1500 standard cubic centimeters per minute (sccm) of hydrogen for all tests and both anode and cathode inlet gas streams were humidified to 100 % relative humidity (dew point temperature) at the cell temperature and inlet pressure. Membrane electrode assemblies were Ion Power (New Castle, DE) catalyst coated Nafion 112 membranes (DuPont, Wilmington, DE) with a catalyst areal density of 0.3 mg cm^{-2} platinum on both anode and cathode. The GDLs used were carbon fiber paper with integral micro-porous layers with a total thickness of 220 μm. Quantitative water content

[a] Certain trade names and company products are mentioned in the text or identified in an illustration in order to adequately specify the experimental procedure and equipment used. In no case does such identification imply recommendation or endorsement by NIST, nor does it imply that the products are necessarily the best available for this purpose.

measurements and images were processed using a dry reference image and background subtraction. In the results presented below, false-color radiographs are shown with darker colors (black, gray, and blue) representing low water thicknesses and light colors (light blue, yellow, red) representing regions of higher water thicknesses. All color images in this paper have the same water thickness scale as shown in Figure 1. The humidified gases were fed in a co-flow arrangement from the inlet in top left corner to the exit at the bottom right corner with gravity acting in the downward direction.

The fuel cell was fitted with a small thermocouple (Omega, k-type) to measure the exit gas temperature at the end of the flow channel for both anode and cathode flows. The 250 μm diameter thermocouple was inserted into the exit flow tube with the tip of the thermocouple located exactly at the exit mouth of the gas flow channel where the four serpentine channels converged. The outlet connections of the anode and cathode gas flow channels external to the cell body were fitted with Vaisala (Helsinki, Finland) HMT337 temperature and dew point meters. The internally heated dew point probe was placed in-line with the exit flow and the surrounding stainless steel tubing was insulated and heated to 5 ºC above the bulk cell temperature set point to avoid condensation effects as the fuel cell product gas exited the cell.

The published specifications for the absolute error for the thermocouples used in this work are +/- 1.1 ºC. At open circuit when the cell was not producing any waste heat, the cell temperature control thermocouple, the humidifier temperatures, and the gas inlet and outlet thermocouple readings were all within 0.5 ºC of one another, indicating that

the differential temperatures between the are likely accurate to +/- 1.5 ºC, which is significantly lower than the approximately 4 ºC to 7 ºC temperature rises observed for the exit flow gas. The error for the Vaisala dew point sensors was +/- 2 % RH which corresponds to an uncertainty in the reported dew points of 0.5 ºC for a gas stream temperature of 60 ºC or and uncertainty of 0.6 ºC in the dew point at 80 ºC. When the cell was at open circuit, the dew points maintained a steady value at the humidifier and cell temperature indicating that the humidifiers were indeed maintaining the dew point of the inlet gases.

In a previous report, the cell water content was expressed in units of mg cm^{-2}.[17] The water contents reported in this work between 0.4 and 0.9 mL per 50 cm^2 active area, correspond to 8 and 18 mg cm^{-2}, which is within the range of that reported previously for simulations of through-plane water content.[18] Since the water content across the cell active area is by no means uniform as confirmed in the images, the total cell water content is reported here simply for comparative purposes. At steady-state (more than 20 min of equilibration), the cell water content fluctuates about ± 1 mg cm^{-2} (0.05 mL) around the mean for conditions similar to this study. The water content fluctuation is most likely due to intermittent expiration of water slugs. The relative uncertainty in total water content has been estimated to be 10 % - 20 % which gives a relative error of ± 0.13 mL for the values reported.

Results and Discussion

The experiments conducted in this study consisted of a long equilibration period at open circuit (at least 20 min), followed by an instantaneous step change in current density from 0 A cm^{-2} to 1.5 A cm^{-2}. The cell parameters of current, voltage, anode and cathode gas outlet temperature, and dew point were recorded over the duration of the experiment. Additionally, temporally-resolved neutron images were collected during the experiments from which the total cell water content could be computed. Shown in Figure 1 are a series of images taken during an experiment at 80 ºC bulk cell temperature and two stoichiometry cathode flow, along with a plot of the total cell water content as a function of time. In the radiographs, significant buildup and expiration of liquid water slugs was observed near the bottom (outlet) of the cell. Only the last 10 % of the cell active area seemed to contain long slugs that span approximately one-half the length of a channel pass, about 3 cm to 4 cm. An instantaneous step change in the current density at 120 s (Figure 2) was followed by an initial rapid increase in water content, then a slowing of the increase. At about 400 s (280 s after the current step change), the total water content began to reach a plateau. From this point until the end of the experiment, the liquid water content fluctuated around 0.43 mL, with the fluctuations being primarily due to slug advection near the bottom of the cell. The cell current and voltage output for two and four stoichiometry cathode flow experiments at 80 ºC are shown in Figure 2. As anticipated, the cell potential was higher at 1.5 A cm^{-2} for four stoichiometry cathode flow and stabilized more quickly than at two stoichiometry. The cell potential at two stoichiometry cathode flow is fairly stable after coming to equilibrium, however, there is some variation as 1.5 A cm^{-2} is close to the limiting current of the cell under these

conditions, and the periodic expiration of liquid water slugs may have had a slight effect on the cell electrical output.

The total cell water content as a function of time is shown in Figure 3 for both the two and four stoichiometry cases at a cell temperature of 80 ºC. The four stoichiometry case is numbered to indicate the points at which images are shown in Figure 4. The water contents were relatively similar for the two cases due to evaporation being the dominant water removal mechanism under these conditions, e.g. slug advection was not influenced much by the increased gas velocity at four stoichiometry.[19] It is also interesting to observe the dry inlet region at the top of the cell for both two and four stoichiometry gas flow cases. At two stoichiometry cathode flow, the darker, dry region is larger than for the four stoichiometry case. In a previous report,[17] the area of the dry inlet region was analyzed by considering the heating of the cell due to the cell load and a subsequent drop in the local relative humidity. Condensation of liquid water (as indicated by lighter, blue colors) did not occur until the cathode gas stream reached saturation from the cell reaction product water. This drying effect caused by local heating was at play in the experiments reported herein where the greater air flow in the four stoichiometry case caused cooling of the cell and a subsequently smaller dry region at the top of the cell. The fluctuations in water content appear equal to or greater for the four stoichiometry case than for the two stoichiometry case due to this cooling effect even though the cell potential is steadier for the four stoichiometry case. The fluctuations in water content observed at four stoichiometry could be due to more slug formation at the lower cathode gas temperature, or more of the cell area containing water slugs where slug expirations

could causes greater fluctuations. Under the conditions in these experiments at 80 ºC, which are typical of many laboratory fuel cell studies, this type of relationship between water content and cell potential, e.g. fluctuating water content while relatively steady potential, especially at four stoichiometry, may indicate that the diffusive resistance of oxygen transport through the porous transport media (gas diffusion layer and microporous layer) to the cathode catalyst layer is more important than the dynamic behavior of the liquid water slugs. Therefore, the presence of water at high stoichiometry does not have a big influence on the performance, but still may contribute to local reactant starvation or water swelling causing increased degradation in those areas of the cell that are observed to contain more water, even with the higher gas flow rate where one would assume that the cell is under relatively little stress.

Figure 5 shows the anode and cathode cell outlet temperatures and outlet dew points for the two and four stoichiometry cases at a cell control temperature of 80 ºC. Panel (a) in Figure 5 shows that the gas flow channel outlet temperatures are significantly lower for the four stoichiometry case due to the greater heat removal by the higher mass flow rate (the gas enters at 80 ºC and is warmed by the waste heat of the cell reaction). The two large temperature excursions of the cathode outlet temperature for the four stoichiometry case correspond to times of relatively low water cell water content (Figure 3). These temperature excursions could have been due to large water slugs clearing the cell possibly as a result of a droplet entering the cell at 80 ºC from the gas inlets, even though heated knockout drums were used at the inlets to avoid introducing liquid water directly into the cell. The temperatures of the anode and cathode for both cases were

similar indicating that the heat exchange between the anode and cathode compartments was rapid. The dew points of the anode and cathode shown in Figure 5(b) diverged for both two and four stoichiometry cases after the step change to 1.5 A cm^{-2} was initiated. The anode dew point for both cases declined indicating that the anode outlet gas was becoming less saturated as the experiment progressed. The cathode dew point for both cases rose quickly in accordance with the water production by the oxygen reduction reaction and temperature rise when the step was initiated. Interestingly, the time scales over which the anode and cathode dew points changed was different. The anode dew point declined on a slower time scale than either the temperature rise or the increase in cathode dew point. This different time scale behavior could indicate that water transport mechanisms that function at the anode, e.g. advection of water from the porous transport media and electro-osmotic drag, which remove water from the anode side of the cell, are slower than water generation and buildup at the cathode. Also, since the anode dew point was less than the exit cell temperature, the anode side of the cell was not completely saturated once the current step was initiated. Since water is produced on the cathode side of the cell, the dew point can change rapidly and given the temperature and dew point information seems to be almost completely saturated upon exit of the cell.

At 60 ºC for the same cathode flow conditions of two and four stoichiometry, the liquid water content in the active area of the cell was significantly greater than for the 80 ºC case, which supports previous work.[17,20] Figure 6 displays the water content as a function of time for two and four stoichiometry cathode flow cases at 60 ºC and images for the points as noted on each plot. The dry inlet regions were smaller for the 60 ºC case

when compared to the 80 ºC data, and again, the cooling afforded by the four stoichiometry cathode flow decreased the area of the dry inlet versus two stoichiometry flow. Accompanying the increased total cell water content, more significant water buildup occurred in the bottom portion of the cell. Slugs extended the width of the cell or longer, whereas at 80 ºC, the slugs tended to be shorter (one-half the width of the cell or less). The cell current and voltage performance along with the water content for both two and four cathode flow stoichiometry cases at 60 ºC is shown in Figure 7. Under these conditions, the high water contents in the cell caused voltage excursions to low potentials indicating that the cell was near collapse. In fact, in the case of four stoichiometry, the voltage began to decline as the cell water content was building up between 700 s to 1000 s and there was no sign of cell recovery before the test was completed.

The voltage excursions for both cases occurred when the total cell water content was about 0.8 mL to 0.9 mL or greater across the entire 50 cm^2 active area. This total cell water content corresponds to 16 to 18 mg cm^{-2} of liquid water in the active area. As elucidated previously and shown in Figure 6 in Ref. 17, the water content of the cell is not at its maximum under high current density operation. Previous work has shown that the maximum water content in the cell is achieved at intermediate current densities – between 0.25 and 1.0 A cm^{-2} (the exact point depending on the cell temperature and flow conditions), where the water production is balanced with the local heating of the cell. Catastrophic flooding occurred at a cell water content of 22 mg cm^{-2} or about 1.1 mL of total water where the water slugs were extended nearly all the way across a channel run.

The outlet temperatures and dew points for the 60 ºC case are shown in Figure 8. A similar trend was observed as with the 80 ºC case, where the anode and cathode temperatures increased after the step change, the cathode dew point increased, and the anode dew point declined. The temperatures with four stoichiometry cathode flow were lower than those for two stoichiometry, demonstrating that increased cooling resulted from the higher flow. The temperature profiles provide some rationale as to why the cell showed catastrophic flooding behavior with four stoichiometry cathode flow while only transient events were recorded at two stoichiometry cathode flow. The slightly lower temperature of the cathode outlet gas, approximately 2 ºC to 3 ºC, with four stoichiometry flow was enough to suppress water removal by evaporation which led to cell flooding and collapse. The slightly higher temperature of the anode and cathode in the two stoichiometry flow case were enough to prevent a runaway flooding event from occurring. As the cell voltage dipped, enough additional heat was produced to cause evaporation within the cell and allow for recovery of the cell. This performance behavior shows that both evaporative removal and liquid water slug advection[21] are important mechanisms in maintaining cell performance at high current densities. Moreover, the exact details of water removal depend on the bulk cell temperature, gas flow rate, and local heating by the cell load.

While not a specific focus of this work, the large amount of water observed near the outlets of the cell is a concern for long-term aging effects of the membrane electrode assembly. Liquid water slugs can cause fuel starvation, leading to accelerated catalyst corrosion,[22] and cyclic swelling stresses on the membrane under hydration/dehydration conditions.[23] Often times, it is assumed in laboratory single-cell studies, that high

stoichiometry gas flow and high inlet humidity, places the cell in an operational space that is relatively mild. The experiments reported here show that considerable liquid water buildup occurs in the bottom 10 % to 20 % of the cell under what might be considered benign conditions. This data on the liquid water location may help to shed light on degradation studies on large cells where they may be differences in the degradation processes across the area of the cell.

Conclusions

Transient flooding events were imaged using neutron radiography while simultaneously recording cell performance. Higher cathode inlet gas flow rates (four stoichiometry) led to lower total cell water content than for cases with lower cathode inlet gas flow rates (two stoichiometry). At 80 ºC, the expected trends were observed with a greater and steadier voltage with four stoichiometry cathode flow, while there was some small fluctuation at two stoichiometry due to intermittent liquid water slug buildup and removal. The outlet gas temperatures of both the anode and cathode increased quickly as the current was changed instantaneously from 0 A cm^{-2} to 1.5 A cm^{-2}. The dew point of the cathode gas increased while the dew point of the anode gas stream decreased indicating that water was transferred away from the anode under the conditions of the study.

Interestingly, at a cell temperature of 60 ºC when the cathode flow rate was increased from two to four stoichiometry, the additional cooling from the incoming gas flows caused more severe flooding, even though water slug advection should have occurred more readily at the higher flow rate. This connection between the cell temperature due to local heating and water removal by gas flow shearing underscores the importance of considering the coupled nature of the heat and water transport and removal during the operation of proton exchange membrane fuel cells under a variety of conditions where water can be removed in either the liquid or gaseous phases. Catastrophic flooding was observed at 60 ºC and four stoichiometry where the large current and convective cooling of the inlet gas produced large slugs in the outlet portion of the cell.

Acknowledgements

Sandia is a multiprogram laboratory operated by Sandia Corporation, a Lockheed Martin Company, for the United States Department of Energy's National Nuclear Security Administration under contract DE-AC04-94AL85000. This work was supported by Sandia National Laboratories Laboratory Directed Research and Development (LDRD) program, the Penn State Institutes of Energy and the Environment, the Penn State Materials Research Institute, the U.S. Department of Commerce, the NIST Ionizing Radiation Division, the Director's office of NIST, the NIST Center for Neutron Research, and the Department of Energy through interagency agreement no. DE-AI01-01EE50660.

References

1. C.-Y. Wang, *Chem. Rev.*, **104**, 4727 (2004).

2. M. A. Hickner, N. P. Siegel, K. S. Chen, D. S. Hussey, D. L. Jacobson, and M. Arif, *J. Electrochem. Soc.*, **155**, B427 (2008).

3. J. P. Owejan, T. A. Trabold, D. L. Jacobson, M. Arif, and S. G. Kandlikar, *Int. J. Hydrogen Energy*, **32**(17), 4489 (2007).

4. I. A. Schneider, D. Kramer, A. Wokaun, and G. G. Scherer, *Electrochem. Comm.* **7**, 1393 (2005).

5. D. Spernjak, S. G. Advani, and A. K. Prasad, *J. Electrochem. Soc.*, **156**, B109 (2009).

6. P. Boillat, G. G. Scherer, A. Wokaun, G. Frei, and E. H. Lehmann, *Electrochem. Comm.* **10**(9), 1311 (2008).

7. C. Hartnig, I. Manke, R. Kuhn, S. Kleinau, J. Goebbels, and J. Banhart, *J. Power Sources*, **188**(2), 468 (2009).

8. P. P. Mukherjee and C.-Y. Wang, *J. Electrochem. Soc.*, **154**, B1121 (2007).

9. A. Z. Weber and J. Newman, *J. Electrochem. Soc.*, **153**, A2205 (2006).

10. R. M. Moore, K. H. Hauer, G. Randolf, and M. Virji, *J. Power Sources*, **162**, 302 (2006).

11. G. Maranzana, O. Lottin, T. Colinart, S. Chupin, and S. Didierjean, *J. Power Sources*, **180**(2), 748 (2008).

12. D. Gerteisen, T. Heilmann, and C. Ziegler, *J. Power Sources*, **187**(1), 165 (2009).

13. Y. Wang and C.-Y. Wang, *J. Electrochem. Soc.*, **154**, B636 (2007).

14. X. Zhu, P. C. Sui, and N. Djilali, *Microfluidics and Nanofluidics*, **4**(6), 543 (2008).

15. K. S. Chen, *Proceeding of the ASME 6th International Fuel Cell Science, Engineering & Technology Conference*, FUELCELL2008-65137 (2008).

16. X. G. Yang, F. Y. Zhang, A. L. Lubawy, and C.-Y. Wang, *Electrochem. Solid-State Lett.*, **7**, A408 (2004).

17. M. A. Hickner, N. P. Siegel, K. S. Chen, D. S. Hussey, D. L. Jacobson, and M. Arif, *J. Electrochem. Soc.*, **155**, B294 (2008).

18. H. Ju, G. Luo, and C.-Y. Wang, *J. Electrochem. Soc.*, **154**, B218 (2007).

19. A. Z.Weber and M. A. Hickner, *Electrochim. Acta*, 53, 7668 (2008).

20. M. A. Hickner, N. P. Siegel, K. S. Chen, D. N. McBrayer, D. S. Hussey, D. L. Jacobson, and M. Arif, *J. Electrochem. Soc.*, **153**, A902 (2006).

21. K. S. Chen, M. A. Hickner, and D. R. Noble, *Int. J. Energy Res.*, **29**, 1113 (2005).

22. J. P. Meyers and R. M. Darling, *J. Electrochem. Soc.*, **153**, A1432 (2006).

23. V. A. Sethuraman, J. W. Weidner, A. T. Haug, and L. V. Protsailo, *J. Electrochem. Soc.*, **155**, B119 (2008).

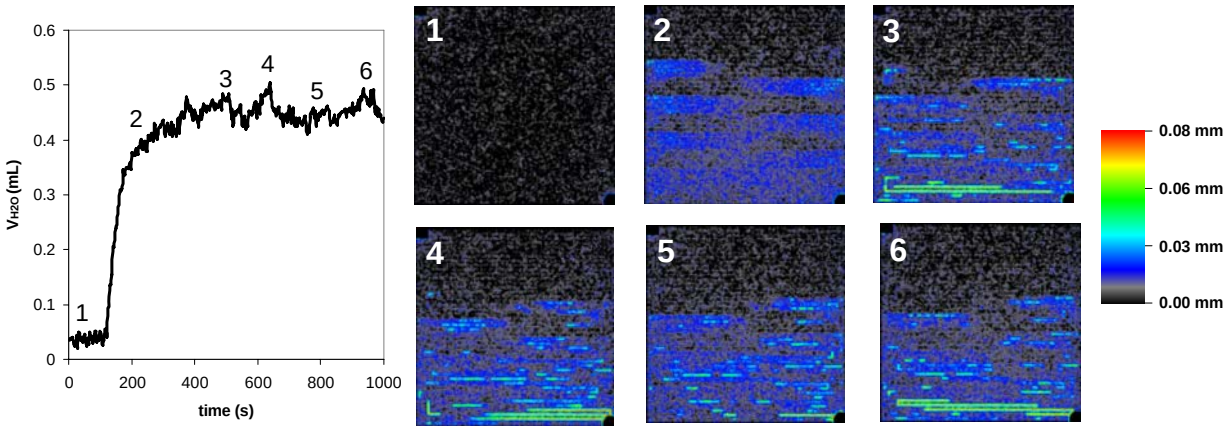

Figure 1. Cell water content and false-color neutron images as a function of time during a step change in cell current density from 0 A cm^{-2} to 1.5 A cm^{-2} initiated at 120 s. Cell temperature was 80 ºC with two stoichiometry cathode flow.

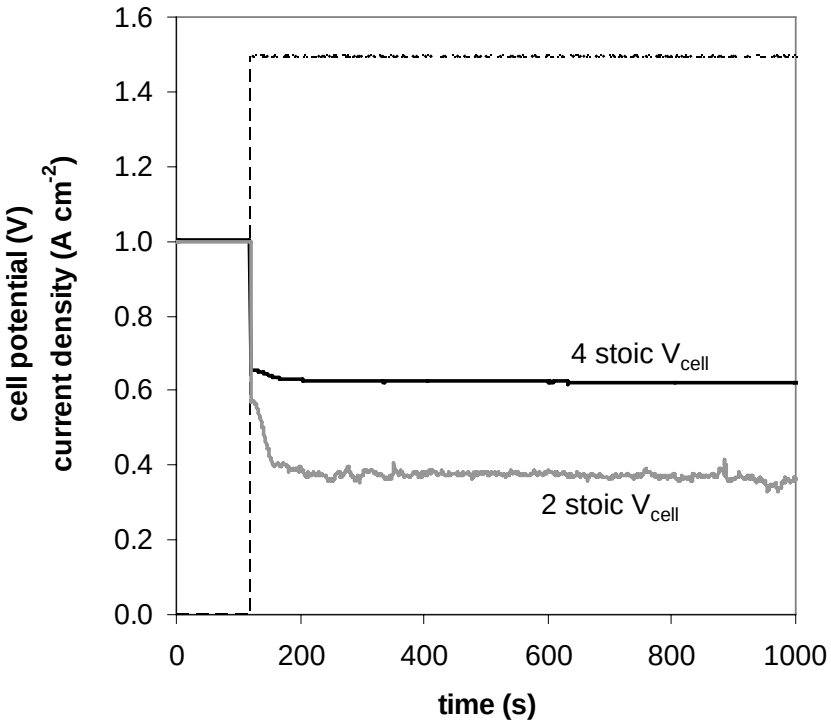

Figure 2. Cell potential and current density (actual data shown for step change) during step change experiments for 80 ºC cell temperature at two and four stoichiometry cathode flows, respectively.

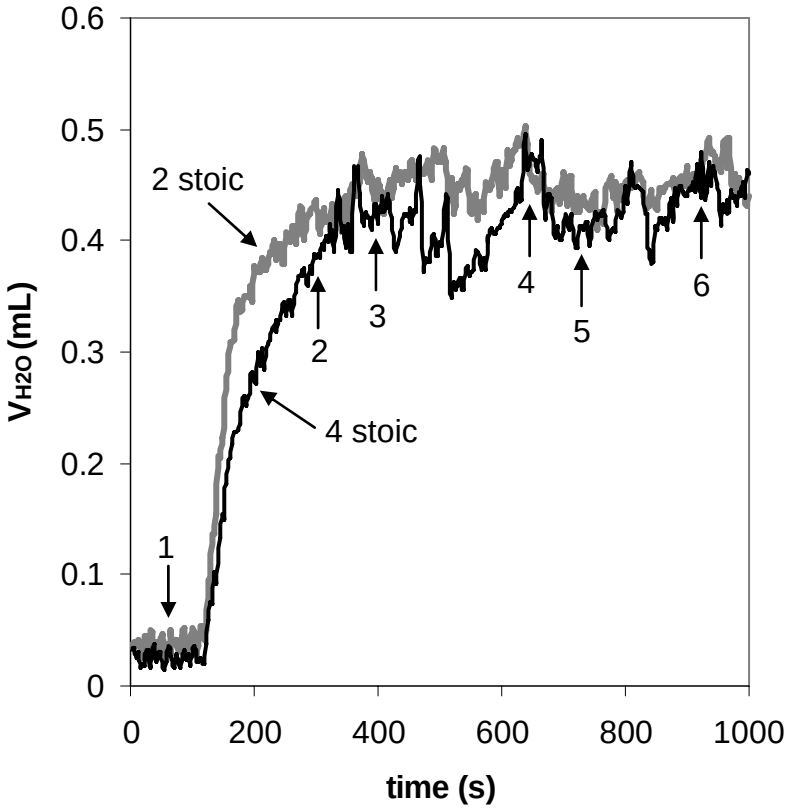

Figure 3. Liquid water volume for two and four stoichiometry cathode flow as a function of time during a step change in current density from 0 A cm^{-2} to 1.5 A cm^{-2} at a cell temperature at 80 ºC. Numbers on plot indicate the points in Figure 4 for which images are shown for the four stoichiometry case.

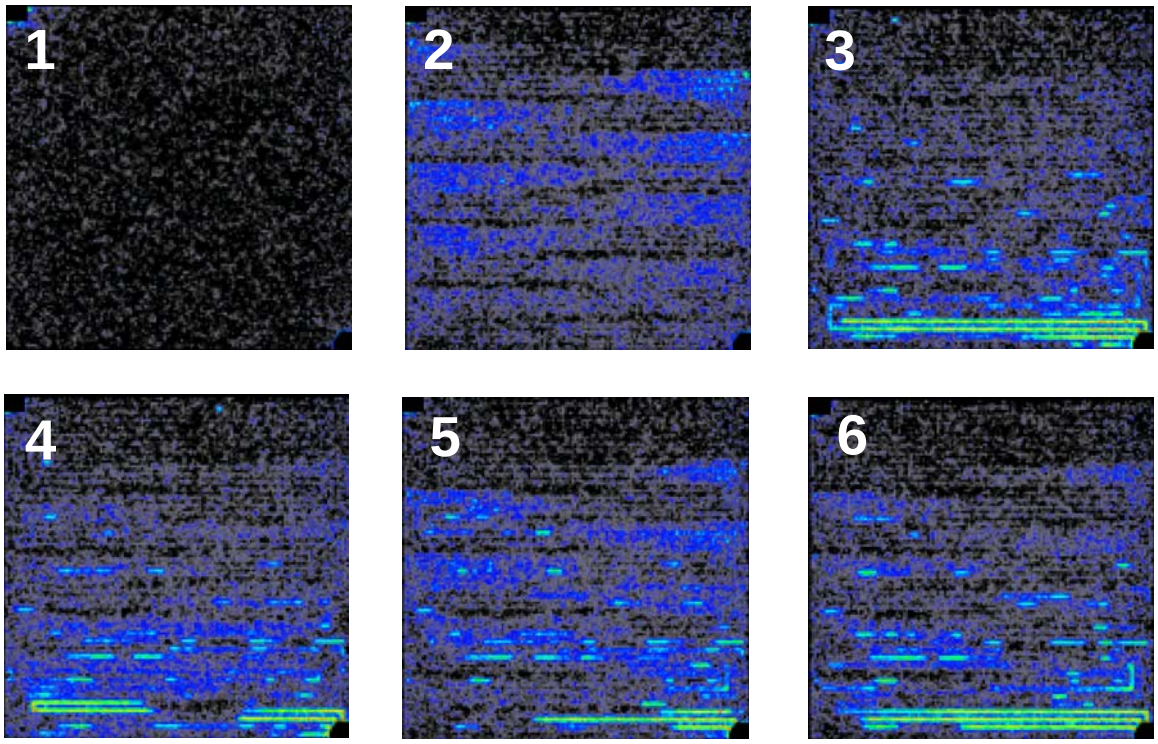

Figure 4. Neutron images showing the active area of a 50 cm^2 at 80 ºC with four stoichiometry cathode flow during a step change in current density from 0 A cm^{-2} to 1.5 A cm^{-2}. Images are numbered corresponding to the arrows in Figure 3.

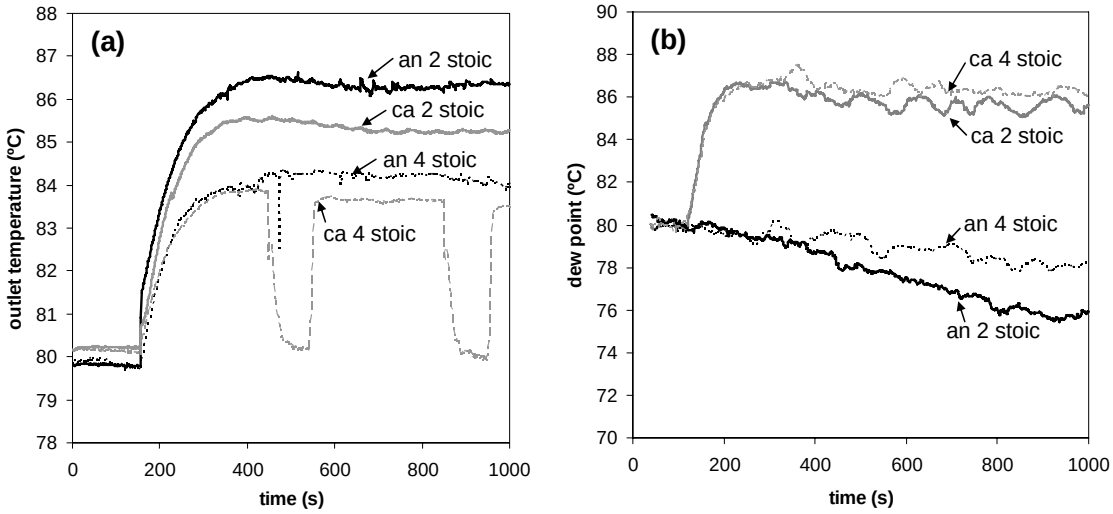

Figure 5. Anode (an) and cathode (ca) (a) outlet temperatures and (b) dewpoints during a step change in current density from 0 A cm^{-2} to 1.5 A cm^{-2} at 120 s for a cell control temperature of 80 ºC.

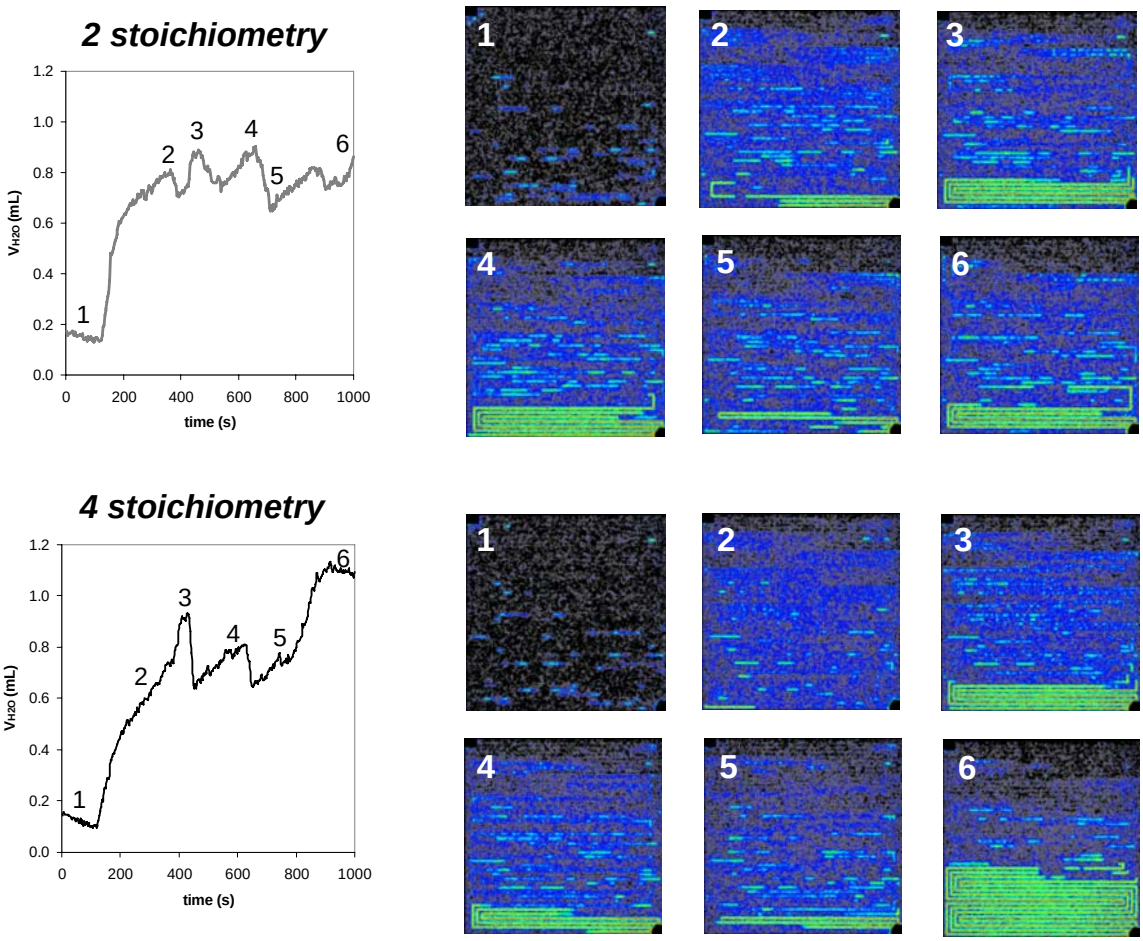

Figure 6. Water content as a function of time and cell neutron images for 60 ºC cell temperature and two and four stoichiometry cathode flows.

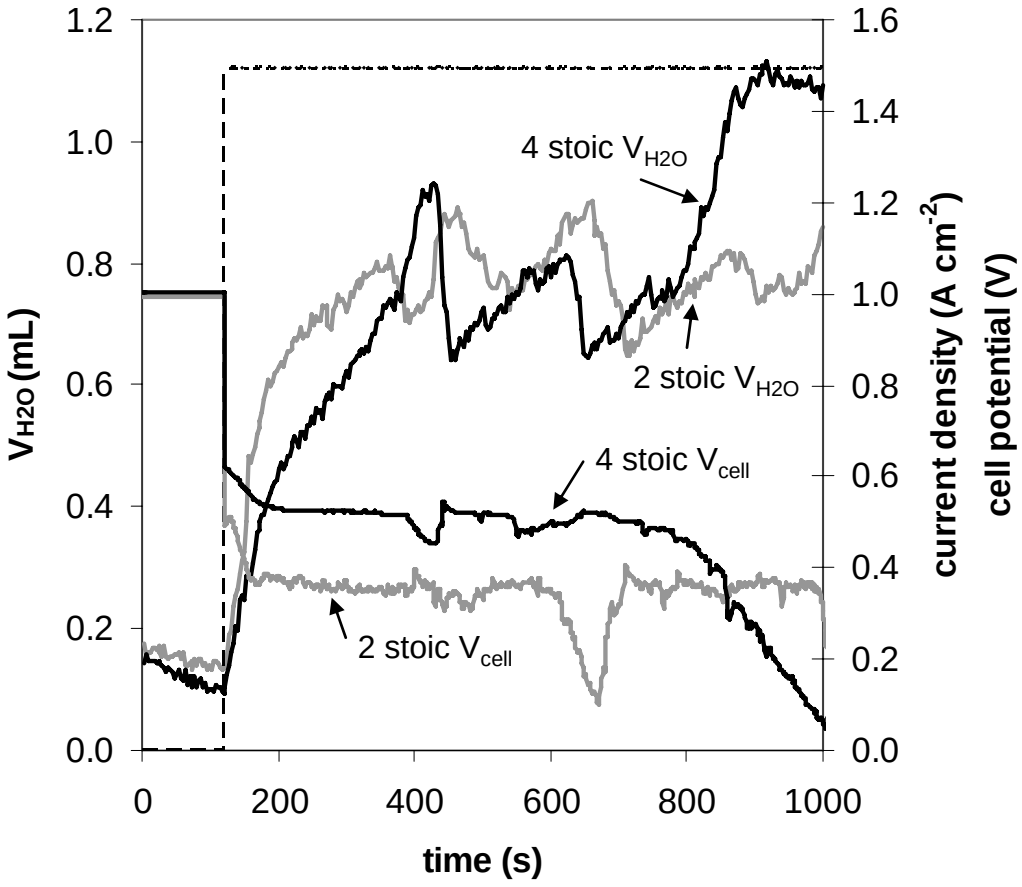

Figure 7. Liquid water volume, cell potential, and current density (actual step change data shown) for 60 ºC cell temperature at two and four stoichiometry cathode flows showing real-time flooding and voltage excursion events.

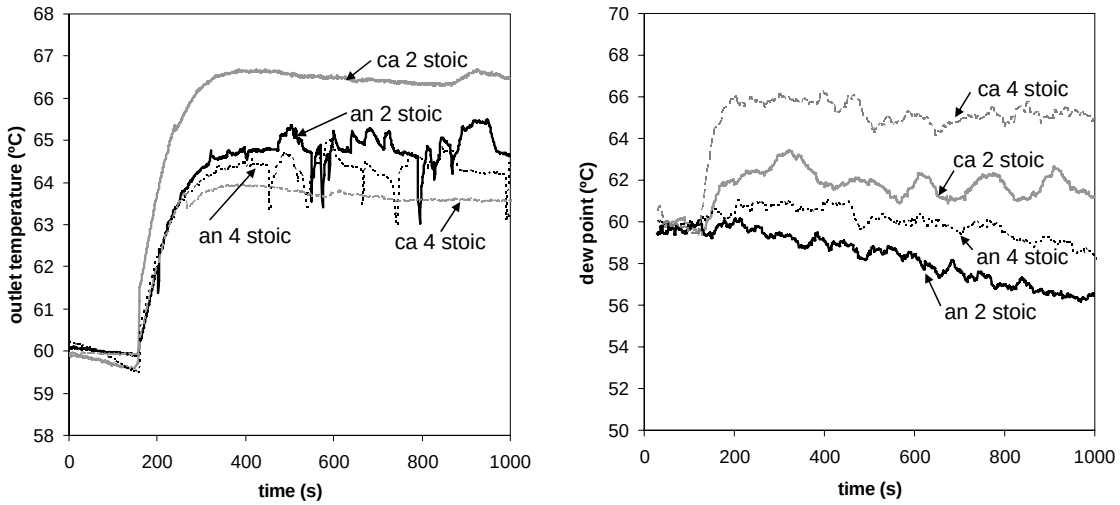

Figure 8. Anode (an) and cathode (ca) (a) outlet temperatures and (b) dew points during a step change in current density from 0 A cm^{-2} to 1.5 A cm^{-2} at 120 s for a cell control temperature of 60 ºC.